ORIENTAL JOURNAL OF CHEMISTRY
An International Open Access, Peer Reviewed Research Journal
www.orientjchem.org
ISSN: 0970-020 X
CODEN: OJCHEG
2025, Vol. 41, No.(2):
Pg. 425-432

Stability and Scalability of $Na_3V_2(PO_4)_4$ Cathode Material for Next-Generation Sodium-Ion Batteries

PRADEEP KUMAR[1], SANJU CHOUDHARI[1], MANISHA YADAV[1], SANTOSH KUMAR[1], HANSRAJ SHARMA[2] and PURA RAM[1]*

[1]EMD laboratory, Department of Physics, University of Rajasthan, Jaipur 302004, Rajasthan, India.
[2]Thin Film and Energy Science Lab, Department of Physics, University of Rajasthan, Jaipur 302004, Rajasthan, India.
*Corresponding author E-mail: puraram@gmail.com

http://dx.doi.org/10.13005/ojc/410211

(Received: January 21, 2025; Accepted: March 08, 2025)

ABSTRACT

This research focuses on the synthesis and characterization of $Na_3V_2(PO_4)_3$ (NVP) as a cathode material for sodium-ion battery (SIB). A sol-gel technique was used to synthesize NVP nanoparticles as electrode materials for SIBs. The synthesized materials include pristine NVP-1, a stored sample (NVP-2) to examine time-induced degradation or structural stability, and NVP-3, a bulk sample (10×scale) for large-scale production analysis. The creation of a rhombohedral NASICON-type structure (R3c space group) is confirmed by XRD with minimal lattice distortion. Thermogravimetric analysis (TGA) highlights the material's stability, with weight loss attributed to water evaporation and carbon combustion. Vanadium and phosphate ions' oxidation states are confirmed using X-ray photoelectron spectroscopy (XPS). Surface morphology, analyzed using FE-SEM, reveals nano-sized particles with some agglomeration, influencing electrolyte penetration and ion transport. A comparative analysis of stored and fresh samples reveals subtle structural shifts without phase changes, indicating robust long-term stability. The calculated crystallite size and c/2a ratio align with standard values, reflecting minimal strain and efficient Na diffusion. This comprehensive study demonstrates that NVP offers excellent phase stability and structural potential, giving it the potential to be used in energy storage systems of the future.

Keywords: Sodium-ion batteries, $Na_3V_2(PO_3)_4$, NASICON structure, Thermal stability, Surface morphology, Electrochemical performance, Crystallite size.

INTRODUCTION

Sodium-ion batteries (SIBs) are a viable alternative to lithium-ion batteries (LIBs) due to the availability and affordability of sodium resources, particularly for large-scale energy storage systems. The materials utilized for SIBs are not only abundant but also safe and economical, This makes them very appealing for real-world uses in energy storage technologies that are renewable[1–3]. The markets for electric cars and portable devices are dominated by LIBs because of their high energy density, long cycle life and safety; nevertheless the rising costs and limited availability of lithium reserves pose significant challenges for large-scale

This is an Open Access article licensed under a Creative Commons license: Attribution 4.0 International (CC- BY).
Published by Oriental Scientific Publishing Company © 2018

implementation[4,5]. Therefore, the development of alternate energy storage systems that provide comparable performance at reduced costs. In this context, SIBs have garnered increasing attention as a promising solution. Leveraging sodium's widespread availability and low cost, researchers have made substantial progress in improving the efficiency, cycling stability, and overall performance of SIBs[6,7]. Notably, NASICON-structured materials such as $Na_3V_2(PO_4)_3$ have demonstrated great potential as advanced cathode materials, owing to their superior electrochemical stability and ion conductivity. Moreover, innovations in doping techniques and material fabrication, including improving the Na-ion conductivity of electrolytes based on NASICON, have further driven the development of high-performance SIBs. Despite the progress made in sodium-ion batteries (SIBs), their practical application remains challenging. One of the major obstacles is Finding appropriate electrode materials, especially cathode materials, that can offer quick ion diffusion paths for steady Na^+ insertion and extraction is challenging due to the higher ionic radius of Na^+ than Li^+ (0.98 Å vs. 0.69 Å)[8,9]. The structural degradation that occurs during the intercalation and deintercalation processes is exacerbated by this difference in ionic size. and lowers the ion diffusion coefficient, further complicating the development of high-performance electrode materials. Identifying electrode materials with superior performance is significantly more challenging for SIBs than for lithium-ion batteries (LIBs). The larger size of Na not only hampers the diffusion kinetics but also increases the stress on the electrode structure, leading to rapid capacity fading and reduced cycling stability. Consequently, achieving durable and efficient SIBs requires innovative approaches to material design and optimization to overcome these inherent limitations[10,11].

The use of layered transition metal oxides[12,13], metal hexacyanometalates[14,15], and polyanionic compounds[16,17] as cathode materials has been widely investigated in recent years. Among these, $Na_3V_2(PO_4)_3$ (NVP) stands out due to its sodium superionic conductor (NASICON) framework, resulting in superior ionic conductivity by facilitating 3D tunnels for Na^+ insertion/extraction. Additionally, the NVP structure provides high thermal stability, a fast Na^+ diffusion coefficient, and superior structural stability during cycling, making it an ideal candidate for sodium-ion batteries with superior performance. Polyanionic compounds and multilayer metal oxides are examples of cathode materials that have drawn significant attention because of its long cycle life and superior thermal stability. However, organic compounds have low reaction kinetics, and metal oxides frequently undergo charge/discharge cycles that result in irreversible structural alterations. However, polyanionic substances such as NVP, have exceptional electrochemical performance, great structural stability, and rapid Na^+ diffusion[20–24]. Among the cathode materials investigated, NVP is particularly promising due to its unique NASICON framework, It facilitates effective Na^+ diffusion by offering a 3D open network. NVP inserts and removes two sodium ions during the electrochemical process, producing an impressive 3.4 V peak voltage and 117 mAh g^{-1} specific capacity[18,19]. Furthermore, NVP demonstrates a higher energy density of approximately 400 Wh kg^{-1} and remarkable cycling stability, solidifying its capacity as a top cathode substance for SIBs[20–24].

The polyanionic molecular structure $Na_3V_2(PO_4)_3$ (NVP) has NASICON (Na Super Ion Conductor) structure, This makes it a suitable sodium-ion battery cathode component. NVP's distinct three-dimensional structure, formed by corner-sharing VO_6 octahedra and PO_4 tetrahedra, contributes to excellent structural stability and extended cycle life by offering ample interstitial gaps for effective Na-ion diffusion[25,26]. While the sodium ions at Na1 sites maintain a strong interaction with the oxygen atoms, the sodium ions at Na2 sites actively engage in the charge/discharge process[27,28]. NVP's intrinsic disadvantages, including poor rate performance and weak ionic conductivity, persist despite these benefits, require further optimization to meet practical energy storage demands[29]. In this study, we synthesize and characterize $Na_3V_2(PO_4)_3$/C (NVP) as a material for the cathode of sodium-ion batteries (SIBs). A sol-gel technique was used to prepare three NVP samples: pristine NVP-1, stored NVP-2 to assess structural stability over time, and bulk NVP-3 (10×scale) for large-scale production analysis. The results of this study help to develop the advanced, cost-effective and high performing cathode materials for sodium-ion batteries.

EXPERIMENTAL

Chemicals

The electrode material has been synthesized using analytical-grade chemicals, including citric acid, sodium carbonate anhydrous (Na_2CO_3, >99.5%), ammonium phosphate monobasic ($NH_4H_2PO_4$, >98%), and vanadium(V) oxide (V_2O_5, >98%).

Material synthesis

Using the Sol-Gel technique, the porous $Na_3V_2(PO_4)_3$/C (NVP) material was created. Using the standard procedure, a stoichiometric mixture of sodium carbonate (Na_2CO_3), vanadium pentoxide (V_2O_5) and ammonium dihydrogen phosphate ($NH_4H_2PO_4$) was used in molar ratios of 3: 2: 6. Initially, 0.6359 g of Na_2CO_3 and 1.3804 g of $NH_4H_2PO_4$ were dispersed to create Solution A in 20 mL of deionized water., which was stirred at 70°C for 15 minutes. 1.5370 g of citric acid and 0.7275 g of V_2O_5 were dissolved simultaneously in 20 mL of deionized water to generate Solution B. The mixture was then stirring for 30 min at 70°C until it was fully dissolved. A dark blue colloid was produced by progressively adding Solution A to Solution B while stirring constantly for five hours at 80°C. To create a dry precursor gel, this mixture was dried for 24 h at 80°C. The dehydrated item was ground and calcined under flowing argon gas at 750°C for 6 hours. Once naturally cooled to ambient temperature, the final composite was ground into a fine powder. To confirm the scalability and reproducibility of this synthesis process, a bulk synthesis was performed using the same molar ratios but with tenfold increased quantities of each reagent, maintaining identical conditions for stirring, drying, and calcination.

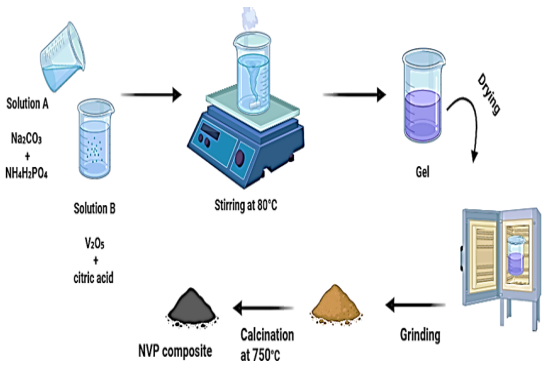

Fig. 1. Scheme of synthesis of NVP sample by sol-gel method. (This work)

Characterization

Electrodes NVP-1, NVP-2, and NVP-3 were structurally and morphologically characterized utilizing a variety of analytical methods. To verify the creation of the NASICON-type structure, Utilizing a Rigaku SMARTLAB system operating at 40 kV voltage and 50 mA current, XRD patterns were recorded using Cu Kα radiation (λ = 1.54184 Å). A Nova Nano FE-SEM 450 was used to analyze the composition and surface morphology, revealing nano-sized particles and flake-like structures with time-dependent changes in porosity. Thermogravimetric analysis (TGA) was performed with a Hitachi model-7300 to evaluate thermal stability, showing minimal weight loss due to moisture and carbon content. Using a Thermo Scientific Nexsa G2 equipment, The oxidation states and chemical composition of the elements inside the NVP structure were determined using XPS.

RESULTS AND DISCUSSION

X-ray diffractogram analysis

The structural characteristics of the synthesized $Na_3V_2(PO_4)_3$/C (NVP) were investigated using XRD. The development of the rhombohedral NASICON-type framework with the R3c space group was verified by indexing the diffraction patterns. Fig. 2(a) shows the diffractograms that were gathered. The prominent peaks at 2θ values of approximately, 14.34°, 20.21°, 23.91°, 28,91°, 31.74°, and 32.26°, 35.81°, 43.51°, 48.44°, 49.18° correspond to the (012) (104) (113) (024) (211) (116) (300) (1010) (315) (042) planes, respectively, With a rhombohedral NASICON framework, The R-3c space group is closely linked to all of the prominent diffraction peaks, confirming the $Na_3V_2(PO_4)_3$ phase. These findings align with the published data (JCPDS 00-062-0345)[30]. The comparison of XRD patterns between NVP-1 and NVP-2 reveals a noticeable shift in the peak positions, particularly for prominent reflections corresponding to the (113), (024), and (116) planes. In NVP 1, these peaks are observed at 23.91°, 28.91°, and 32.26°, while in NVP 2, they appear at 24.04°, 29.03°, and 32.28°, respectively. These small but measurable shifts suggest a change in the lattice parameters, This may be due to the material's gradual structural change or degradation over storage. This shift in peak positions is typically associated with minor lattice distortions rather than a complete phase transformation. The preservation of the overall peak pattern and indexing to the same rhombohedral NASICON-type framework

(R-3c space group) confirms that the material maintains its original phase, suggesting structural stability at a macroscopic level. The XRD pattern of the bulk NVP material, synthesized for large-scale use, shows prominent peaks at 23.77°, 28.73°, and 32.04°, In accordance with the planes (113), (024), and (116). The XRD pattern remained consistent with the standard synthesis, confirming the preservation of phase purity and crystal structure integrity during scale-up. Bulk materials often experience microstructural strain or defects due to larger processing volumes, which may impact ionic conductivity and phase stability. Nonetheless, the retention of key structural features confirms that the bulk material retains the essential $Na_3V_2(PO_4)_3$ phase, making it suitable for practical applications.

To determine the average crystallite size of the synthesized NVP samples, the Debye-Scherrer formula was utilized. The formula is expressed as:

$$D = \frac{0.9 \cdot \lambda}{\beta \cdot cos\theta}$$

Where θ is the angle of diffraction, λ is the X-ray wavelength, and β is the full width half maximum in radians. The calculated average crystallite size for the most intense peak was derived for the NVP samples using their respective FWHM values. The average particle size for NVP-1, NVP-2, and NVP-3 was calculated as 44.22 nm, 40.34 nm, and 49.79 nm, respectively, based on the FWHM values of their most intense peaks.

Table 1: Crystal structure parameters of synthesized NVP materials

Materials	Lattice Parameters a = b (Å)	c (Å)	d spacing for (116) (Å)	Crystallite size by XRD (Å)	FWHM (116) (°)
NVP-1	8.68042	21.81946	2.7706	461	0.187
NVP-2	8.67731	21.62472	2.7693	422	0.205
NVP-3	8.72238	21.79506	2.7893	521	0.166

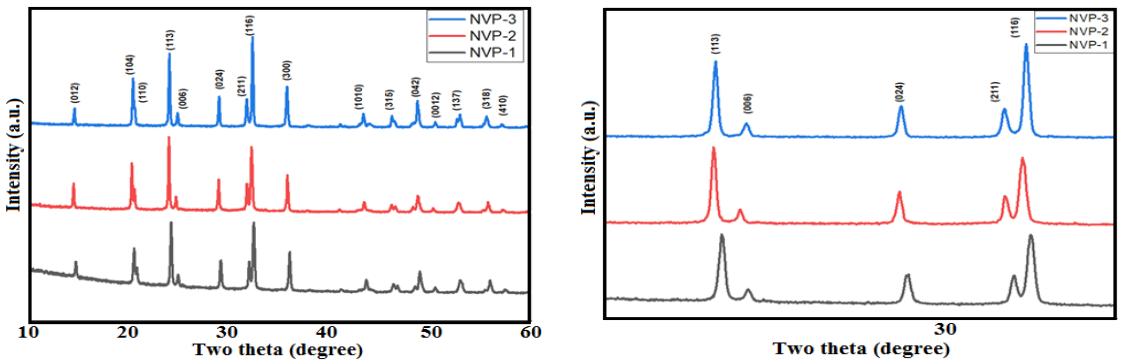

Fig. 2. (a) XRD patterns of NVP-1, NVP-2, NVP-3 (b) expanded view of the (1 1 3), (0 2 4), and (1 1 6) diffraction peaks

Table 2: Based on the lattice constants, the following structural parameters were calculated

Parameter	NVP-1	NVP-2	NVP-3 (Bulk)	JCPDS 00-062-0345
c/2a Tetragonal Distortion	1.246	1.257	1.249	1.249
(D = 2-(c/a))	-0.492	-0.514	-0.499	-0.498
Volume (Å³)	1410.105Å³	1430.187Å³	1436.01Å³	1436.17Å³

The *c/2a* ratio of 1.246, 1.257, 1.249 is within the expected range for NVP and indicates good symmetry and minimal lattice distortion, which is favourable for sodium ion diffusion. The calculated tetragonal distortion values of D = -0.492, -0.514, -0.499 suggest a near-ideal structure. While D ideally should be close to zero to indicate no distortion, the minor negative values observed imply slight lattice distortions. However, the negative value suggests some degree of lattice distortion. For the bulk sample (NVP-3), the c/2a ratio and tetragonal distortion closely align with the JCPDS reference values, reflecting a well-maintained structural symmetry and minimal deviations from the standard NASICON framework. The unit cell volume of the bulk NVP (1436.01Å³) is almost identical to

the JCPDS reference value (1436.17Å^3), indicating a stable and well-ordered crystal structure.

Thermal gravimetric analysis

The NVP samples were subjected to thermogravimetric analysis (TGA) in a nitrogen environment at a scan rate of 15.0°C/min between 27°C and 600°C, as illustrated in Fig. 3. Between 100°C and 200°C, the first weight loss that was noticed was approximately 1.25%, 2.19% and 1.35% for the respective samples, The elimination of water molecules that are weakly bonded or physically adsorbed is the reason behind this. A subsequent weight loss of about 1.11%, 1.34% and 1.10% occurred between 250°C to 500°C, indicating the combustion of carbon species and the partial evacuation of water that was trapped inside the nanoparticles. The weight loss continues at a decreased rate between 400°C and 600°C, which most likely reflects the elimination of residual water from the nanoparticle structure and further combustion of carbon material.[30]

The thermal stability of the NVP samples varies, according to TGA. NVP-1 exhibits the lowest initial weight loss of 1.25%, followed by 1.35% for NVP-3 (Bulk) and the highest 2.19% for NVP-2. The time-delayed sample (NVP-2) shows higher weight loss due to prolonged exposure to environmental conditions, leading to increased absorption of water and potentially more carbon contamination. The subsequent reduction in between 250°C to 500°C is similar for all samples, ranging from 1.10% to 1.34%, reflecting partial removal of water and carbon. However, NVP-3 shows slightly higher overall weight loss, suggesting a greater content of adsorbed water and residual carbon. The thermal stability of NVP-1 and NVP-3 (Bulk) is relatively comparable, while NVP-2 demonstrates a slightly reduced stability due to its higher moisture content.

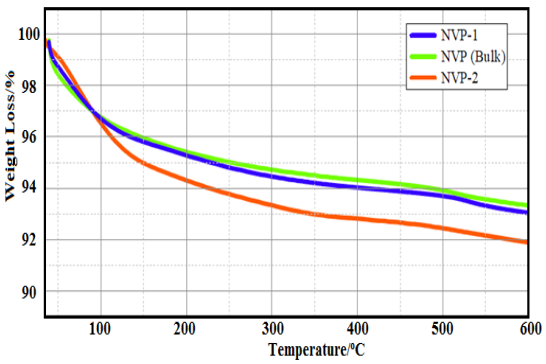

Fig. 3. TGA curve of NVP-1, NVP-2, NVP- (Bulk)

SEM analysis

The synthesized NVP sample's surface morphology was examined utilizing Nova Nano FE-SEM 450 at a magnification of 20,000x. NVP-1 and NVP-3 displays a combination of nano-sized particles and flake-like structures. The nanoparticles exhibit irregular shapes, while the flake structures show thin, layered formations. The agglomeration of particles is noticeable, indicating a tendency for clustering, which could influence the material's electrochemical performance by affecting the active surface area. The NVP-2 shows a transition from distinct nano-flakes to a more compact, porous structure with smoother particles. This change is due to particle aggregation and structural rearrangement over time. Increased porosity enhances electrolyte penetration, while particle aggregation and structural rearrangement affect surface area and ion transport, influencing electrochemical performance.

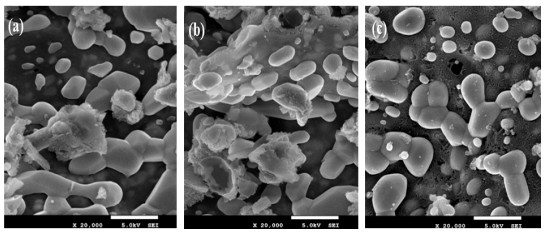

Fig. 4. SEM images of (a) NVP-1 (b) NVP-2 (c) NVP-3

The estimated particle sizes of all three samples range from 40 to 50 nm, indicating relatively small dimensions that contribute to an increased surface area. A few nanoparticles exhibit slight agglomeration, forming small clusters. The calculated average particle sizes are 82.21 nm for NVP-1, 78.28 nm for NVP-2, and 85.04 nm for NVP-3. Notably, the average particle size of NVP-2 decreased after six months, suggesting a time-induced effect on the material's morphology, as further confirmed by XRD analysis. The homogeneous composite's production is confirmed by the EDS mapping of NVP-1, which reveals that the particles Na, V, P, and O are uniformly distributed.

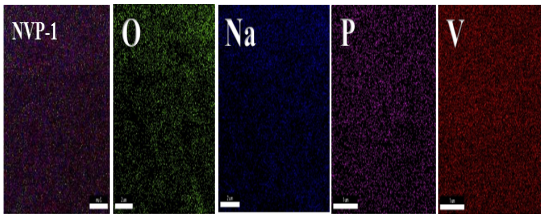

Fig. 5. Elemental composition mapping NVP-1

X-ray photoelectron spectroscopy (XPS)

In order to further examine the element's oxidation states and chemical composition in the $Na_3V_2(PO_4)_3$ (NVP-1). The results of X-ray photoemission spectroscopy (XPS) are displayed in Fig. 6. The Na 1s peak at 1071.4 eV confirms sodium ions in the structure, while the P 2p peak at 133.3 eV corresponds to phosphorus in the +5 oxidation state within phosphate groups. The oxygen in PO_4^{3-} is liable for the O 1s peak at 531.0 eV, while adventitious carbon pollution is the cause of the C 1s peak at 285.0 eV. The V 2p spectrum exhibits peaks at 523.5 eV and 516.6 eV, corresponding to V $2p_{1/2}$ and V $2p_{3/2}$, confirming vanadium in the +3 oxidation state. This analysis verifies the formation of a stable vanadium phosphate framework, essential for efficient sodium-ion storage and transport[31-33].

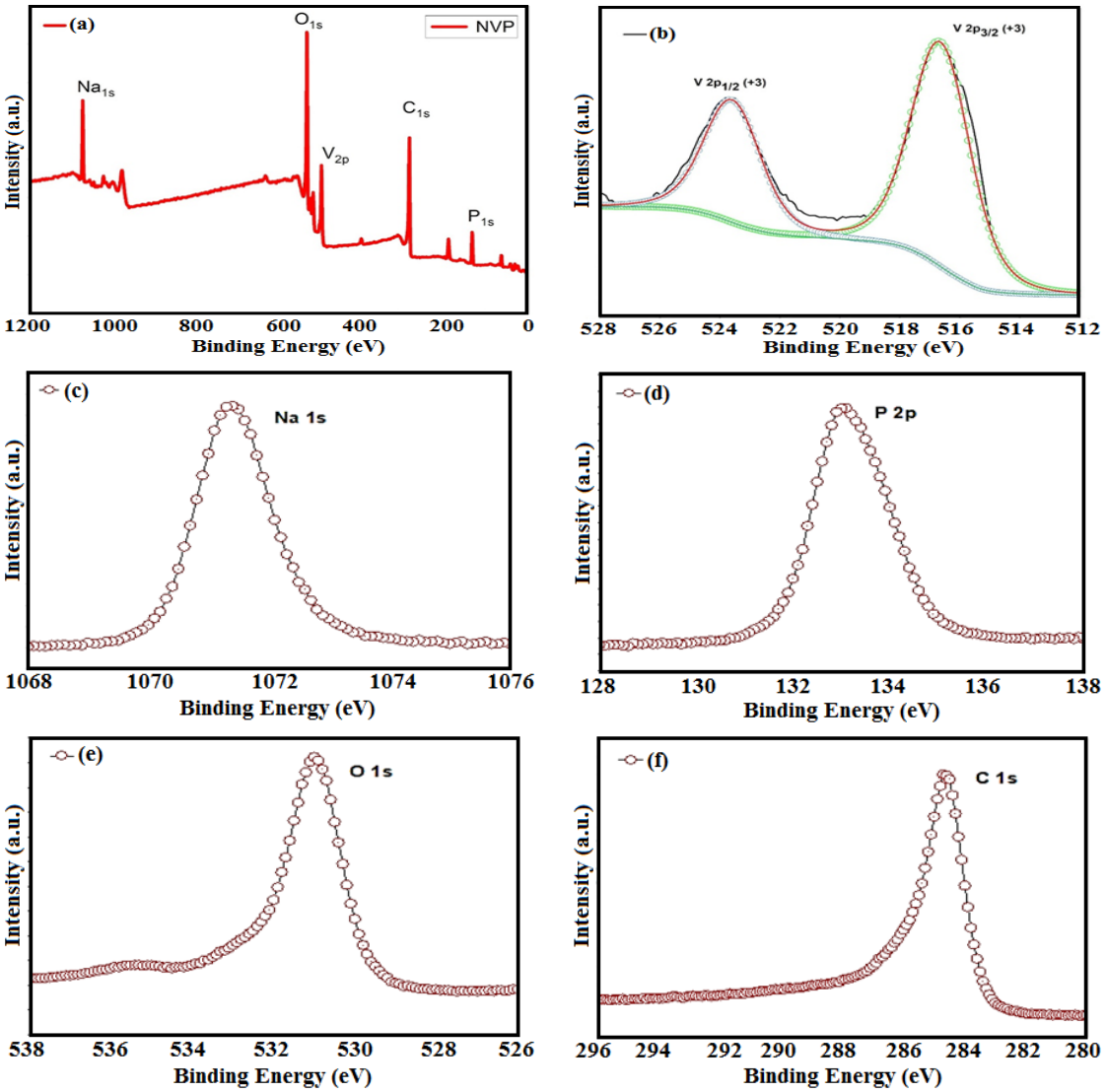

Fig. 6. XPS spectra (a) full spectra of NVP (b) V 2p of NVP sample (c) Na 1s NVP sample, (d) P 2p of NVP sample, (e) O 1s NVP sample (f) C 1s NVP sample

CONCLUSION

In conclusion, $Na_3V_2(PO_4)_3$/C (NVP) materials were successfully synthesized using the sol-gel method, a cost-effective and scalable technique suitable for large-scale production. XRD confirmed the formation of a rhombohedral (NASICON-type) structure with excellent phase purity. The structural stability of NVP-2 demonstrates minor lattice distortions over time, while bulk NVP-3

maintains phase integrity for practical applications. TGA analysis indicates good thermal stability with minimal moisture and carbon content variations. SEM analysis reveals nano-sized particles with time-induced morphological changes affecting porosity and ion transport. XPS verified the presence of Na, P, O, and V in appropriate oxidation states, forming a stable vanadium phosphate framework essential for efficient sodium-ion storage. The sol-gel method's precise control over composition, uniform particle distribution, and reproducibility makes it highly effective for synthesizing superior materials for sodium-ion batteries on a commercial scale.

ACKNOWLEDGMENT

The authors want to acknowledge the University Grants Commission, New Delhi, India for the Ph.D. fellowship and MRC (MNIT, Jaipur), Manipal University (Jaipur), and the Department of Physics (University of Rajasthan, Jaipur) for assisting with the samples' physical characterizations.

Conflict of interest

The authors declare no conflicts of interest regarding the research, authorship, or publication of this paper.

REFERENCES

1. Yabuuchi, N.; Kubota, K.; Dahbi, M.; Komaba, S. Research development on sodium-ion batteries., *Chem. Rev.*, **2014**, *114*, 11636– 11682.
2. Zhang, X.; Rui, X.; Chen, D.; Tan, H.; Yang, D.; Huang, S.; Yu, Y. Na3V2(PO4)3: An advanced cathode for sodium-ion batteries., *Nanoscale.,* **2019**, *11*, 2556–2576.
3. Rao, Y. B.; Bharathi, K. K.; Patro, L. N. Review on the synthesis and doping strategies in enhancing the Na ion conductivity of $Na_3Zr_2Si_2PO_{12}$ (NASICON)-based solid electrolytes., *Solid State Ionics*., **2021**, *366-367*, 115671.
4. An, Q.; Xiong, F.; Wei, Q.; Sheng, J.; He, L.; Ma, D.; Yao, Y.; Mai, L. Nanoflake-assembled hierarchical Na3V2(PO4)3/C microflowers: superior Li storage performance and insertion/extraction mechanism., *Adv. Energy Mater.*, **2015**, *5*, 1401963.
5. Wang, L.; Lu, Y.; Liu, J.; Xu, M.; Cheng, J.; Zhang, D.; Goodenough, J. B. A superior low-cost cathode for a Na-ion battery., *Angew. Chem. Int. Ed.*, **2013**, *52*, 1964–1967.
6. Jiang, Y.; Wu, Y.; Chen, Y.; Qi, Z.; Shi, J.; Gu, L.; Yu, Y. Design nitrogen (N) and sulfur (S) Co-doped 3D graphene network architectures for high-performance sodium storage., *Small.,* **2018**, *14*, 1703471.
7. He, H.; Gan, Q.; Wang, H.; Xu, G.-L.; Zhang, X.; Huang, D.; Fu, F.; Tang, Y.; Amine, K.; Shao, M. Structure-dependent performance of TiO_2/C as anode material for Na-ion batteries., *Nano Energy.,* **2018,** *44*, 217–227.
8. Hou, H.; Banks, C. E.; Jing, M.; Zhang, Y.; Ji, X. Carbon quantum dots and their derivative 3D porous carbon frameworks for sodium-ion batteries with ultralong cycle life., *Adv. Mater.*, **2015**, *27*, 7861–7866.
9. Xu, Y.; Zhou, M.; Wen, L.; Wang, C.; Zhao, H.; Mi, Y.; Liang, L.; Fu, Q.; Wu, M.; Lei, Y. Highly ordered three-dimensional Ni-TiO2 nanoarrays as sodium-ion battery anodes., *Chem. Mater.*, **2015**, *27*, 4274–4280.
10. Palomares, V.; Serras, P.; Villaluenga, I.; Hueso, K. B.; Carretero-Gonzalez, J.; Rojo, T. Na-ion batteries: Recent advances and present challenges to become low-cost energy storage systems., *Energy Environ. Sci.*, **2012**, *5*, 5884–5901.
11. Fang, J. Q.; Wang, S. Q.; Li, Z. T.; Chen, H. B.; Xia, L.; Ding, L. X.; Wang, H. H. Porous $Na_3V_2(PO_4)_3$@C nanoparticles enwrapped in three-dimensional graphene for high-performance sodium-ion batteries., *J. Mater. Chem.* A **2016**, *4*, 1180–1185.
12. Yuan, D. D.; Liang, X. M.; Wu, L.; Cao, Y. L.; Ai, X. P.; Feng, J. W.; Yang, H. X. A honeycomb-layered Na Ni SbO : A high-rate and cycle-stable cathode for sodium-ion batteries., *Adv. Mater.*, **2014**, *26*, 6301–6306.
13. Billaud, J.; Singh, G.; Armstrong, A. R.; Gonzalo, E.; Roddatis, V.; Armand, M.; Rojo, T.; Bruce, P. G. $Na_{0.67}$ Mn_{1-x} $Mg_xO_2(0 \leq x \leq 0.2)$: A high-capacity cathode for sodium-ion batteries., *Energy Environ. Sci.*, **2014**, *7*, 1387–1391.
14. Wessells, C. D.; Huggins, R. A.; Cui, Y. Copper hexacyanoferrate battery electrodes with long cycle life and high power., *Nat. Commun.*, **2011**, *2*, 550.
15. Wessells, C. D.; Peddada, S. V.; Huggins, R. A.; Cui, Y. Nickel hexacyanoferrate nanoparticle electrodes for aqueous sodium and potassium-ion batteries., *Nano Lett.*, **2011**, *11*, 5421.

16. Lee, K. T.; Ramesh, T.; Nan, F.; Botton, G.; Nazar, L. F. Topochemical synthesis of sodium metal phosphate olivines for sodium-ion batteries., *Chem. Mater.*, **2011**, *23*, 3593–3600.
17. Shakoor, R.; Seo, D.-H.; Kim, H.; Park, Y.-U.; Kim, J.; Kim, S.-W.; Gwon, H.; Lee, S.; Kang, K. A combined first-principles and experimental study on Na V (PO) F for rechargeable Na batteries., *J. Mater. Chem.,* **2012**, *22*, 20535–20541.
18. Chen, Y.; Xu, Y.; Sun, X.; Zhang, B.; He, S.; Li, L.; Wang, C. Preventing structural degradation from Na V (PO) to V (PO) : F-doped Na V (PO) /C cathode composite with stable lifetime for sodium-ion batteries., *J. Power Sources.,* **2018**, *378*, 423–432.
19. Jiang, Y.; Yang, Z.; Li, W.; Zeng, L.; Pan, F.; Wang, M.; Wei, X.; Hu, G.; Gu, L.; Yu, Y. Nanoconfined carbon-coated Na V (PO) particles in mesoporous carbon enabling ultralong cycle life for sodium-ion batteries., *Adv. Energy Mater.*, **2015**, *5*, 1402104.
20. Jian, Z.; Han, W.; Lu, X.; Yang, H.; Hu, Y.-S.; Zhou, J.; Zhou, Z.; Li, J.; Chen, W.; Chen, D.; Chen, L. Superior electrochemical performance and storage mechanism of $Na_3V_2(PO_4)_3$ cathode for room-temperature sodium-ion batteries., *Adv. Energy Mater.*, **2013**, *3*, 156–160.
21. Fang, Y.; Xiao, L.; Ai, X.; Cao, Y.; Yang, H. Hierarchical carbon framework-wrapped $Na_3V_2(PO_4)_3$ as a superior high-rate and extended lifespan cathode for sodium-ion batteries., *Adv. Mater.*, **2015**, *27*, 5895–5900.
22. Zhu, C.; Song, K.; van Aken, P. A.; Maier, J.; Yu, Y. Carbon-coated Na V (PO) embedded in porous carbon matrix: An ultrafast Na-storage cathode with the potential of outperforming Li cathodes., *Nano Lett.*, **2014**, *14*, 2175–2180.
23. Rui, X.; Sun, W.; Wu, C.; Yu, Y.; Yan, Q. An advanced sodium-ion battery composed of carbon-coated Na V (PO) in a porous graphene network., *Adv. Mater.*, **2015**, *27*, 6670–6676.
24. Saravanan, K.; Mason, C. W.; Rudola, A.; Wong, K. H.; Balaya, P. Excellent cycling stability and superior rate capability of $Na_3V_2(PO_4)_3$ for sodium-ion batteries., *Adv. Energy Mater.*, **2013**, *3*, 444–450.
25. Hwang, J. Y.; Myung, S. T.; Sun, Y. K. Sodium-ion batteries: Present and future., *Chem. Soc. Rev.*, **2017**, *46*, 3529–3614.
26. Lyu, Y.; Liu, Y.; Yu, Z. E.; Su, N.; Liu, Y.; Li, W.; Li, Q.; Guo, B.; Liu, B. Recent advances in high energy-density cathode materials for sodium-ion batteries., *Sustain. Mater. Technol.*, **2019**, *21*, No. e00098.
27. Wei, C.; Luo, F.; Zhang, C.; Gao, H.; Niu, J.; Ma, W.; Bai, Y.; Zhang, Z. Voltage window-dependent electrochemical performance and reaction mechanisms of $Na_3V_2(PO_4)_3$ cathode for high-capacity sodium ion batteries., *Ionics.,* **2020**, *26*, 2343–2351.
28. Wang, Q.; Zhang, M.; Zhou, C.; Chen, Y. Concerted ion exchange mechanism for sodium diffusion and its promotion in $Na_3V_2(PO_4)_3$ framework., *J. Phys. Chem.* C., **2018**, *122*, 16649–16654.
29. Zeng, X.; Peng, J.; Guo, Y.; Zhu, H.; Huang, X. Research progress on $Na_3V_2(PO_4)_3$ cathode material of sodium ion battery., *Front. Chem.*, **2020**, *8*, 635.
30. Kate, R. S.; Kadam, S. V.; Kulkarni, M. V.; Deokate, R. J.; Kale, B. B., & Kalubarme, R. S. Highly stable and nanoporous $Na_3V_2(PO_4)_3$@C cathode material for sodium-ion batteries using thermal management., *Journal of Energy Storage.*, **2023**, *74*, 109245.
31. N.K. Nag.; F.E. Massoth, ESCA and gravimetric reduction studies on V/Al_2O_3 and V/SiO_2 catalysts., *J. Catal.*, **1990**, *124*, 127e132.
32. J.X. Wang.; Z.X. Wang.; X. H. Li.; H.J. Guo.; W. Xiao.; S. L. Huang.; Z. J. He.; Comparative investigations of $LiVPO_4F$/C and $Li_3V_2(PO_4)_3$/C synthesized in similar soft chemical route, *J. Solid State Electrochem.*, **2013**, *17*, 1e8.
33. J.-C. Zheng, B. Zhang, Z.H. Yang, Novel synthesis of LiVPO4F cathode material by chemical lithiation and postannealing., *J. Power Sources.,* **2012**, *202*, 380e383.